Cobalt-based alloys for orthopaedic applications studied by electrochemical and XPS analysis

ALEKSANDRA KOCIJAN[1,*], INGRID MILOŠEV[1,2], BORIS PIHLAR[3]
[1]*Jožef Stefan Institute, Department of Physical and Organic Chemistry, Jamova 39, 1000 Ljubljana, Slovenia*
E-mail: Aleksandra.Kocijan@ijs.si
[2]*Valdoltra Orthopaedic Hospital, Jadranska c. 31, 6280 Ankaran, Slovenia*
[3]*Faculty of Chemistry and Chemical Technology, Aškerčeva 5, 1000 Ljubljana, Slovenia*

The composition of the passive layers formed by electrochemical oxidation at different passivation potentials on Co–Cr–Mo and Co–Ni–Cr–Mo alloys in simulated physiological solution (SPS), with and without the complexing agent EDTA, was studied by X-ray photoelectron spectroscopy. Composition as a function of depth, cationic fraction and thickness of the passive film was determined. Chromium oxide is shown to be the major constituent of the passive layer on both Co–Cr–Mo and Co–Ni–Cr–Mo alloys. The minor constituents of the passive layers, Co- and Mo-oxide in the case of Co–Cr–Mo alloy and Ni-, Co- and Mo-oxides in the case of Co–Ni–Cr–Mo alloy, are also located in the outer part of the layer. EDTA affects the formation of the passive layer on each alloy. The content of Co-, Ni- and Mo-oxide in the passive layer is lower in the presence of EDTA, thus indicating increased solubility associated with higher stability constants for complexes of metal cations with EDTA.

Introduction

Co-based alloys have long been used successfully in surgical implant applications because of their superior corrosion and biodegradation-resistance and good mechanical properties, including high ultimate tensile and fatigue strength combined with sufficient elongation after fracture [1]. After a metallic material has been implanted into the human body reactions between its surface and surrounding living tissues occur immediately [2]. Tissue compatibility is governed by the reactions at the initial stage, that is, the adsorption of serum proteins on the implant surface, the attachment, proliferation and differentiation of cells, and later, septic and aseptic loosening [2]. In the course of time, the alloy itself and its corrosion products can react directly with the surrounding tissues, be transported by the bloodstream to distant organs or be partially eliminated by body fluids [2]. Long-term articulation of orthopaedic implants, such as knee or hip, can lead to the production of micro- and sub-micrometre sized metal products [2]. Systemic distribution of metal wear particles has been proved in autopsy studies [3]. They have been detected primarily in lymph nodes and often in liver and spleen [3]. It has been shown recently that the release of cobalt, chromium and nickel may lead to hypersensitivity reaction [4]. Several studies have reported increased metal ion concentrations in serum and urine of patients with loosened metal/polyethylene and even with well functioning metal/metal total hip replacements made of Co-based alloy [5, 6]. Taking into account these consequences of metal release in the human body, it is important to analyse the surface composition of these materials when discussing the issue of tissue compatibility.

Various electrochemical and spectroscopic techniques have been used in studying the corrosion behaviour and surface composition of implant alloys. X-ray photoelectron spectroscopy (XPS) is one of the most appropriate techniques for detailed study of the chemical composition at the surface, the oxidation state of particular elements and in-depth chemical composition when combined with ion sputtering [7–9]. Hanawa *et al*. [7] showed that the surface oxide films on Co–Cr–Mo alloy in various quasi-biological environments were about 2.5 nm thick and contained a large amount of OH^- species. Cobalt was dissolved after immersion in Hank's solution and the surface oxide consisted of chromium oxide containing molybdenum oxide. Moore *et al*. [8] studied the differences between passivated and non-passivated ASTM F-75 alloy by Auger electron spectroscopy and XPS. The general surface character and composition was the same, except for cobalt. Surface cobalt ratios (cobalt/oxygen and cobalt/carbon) were lower for passivated samples due to the increased thickness of the oxide layer over the cobalt-rich regions. Maffiotte *et al*. [9] studied the oxide films formed on Co-based alloy during corrosion tests at high temperature at

*Author to whom all correspondence should be addressed.

pH values of 5.05 and 7.4. In both the cases the corrosion mechanism was characterised by preferential dissolution of cobalt and the formation of a protective chromium oxide film. Other spectroscopic techniques, such as UV-visible [10], IR [11], and Raman [12] spectroscopies, have been used for *in situ* measurements. However, UV-visible spectra do not offer as much structural information as vibrational spectra, whereas IR spectra of samples in aqueous solutions are difficult to collect [12]. Li *et al*. [12] investigated corrosion films on Co–Cr–Mo alloy in biosimulating solutions by surface-enhanced Raman spectroscopy at different potentials. The results were similar to those obtained by XPS [8].

In the present work, the composition, thickness and depth profiles of the oxide films formed on Co–Cr–Mo and Co–Ni–Cr–Mo alloys were studied by XPS analysis in simulated physiological solution (SPS), pH = 7.8, at various potentials. The complexing agent EDTA simulated the influence of biomolecules, which *in vivo* act as complexing agents for metal ions and play an important role in the corrosion process.

Materials and methods

The alloys were cut from original orthopaedic prostheses (Protek AG, Bern, Switzerland). Alloy composition was confirmed by energy dispersive X-ray analysis (EDA) as follows: Co–Cr–Mo alloy (cast Protasul-1, ASTM F75-87 [13]) 27.9 at % Cr, 3.4 at % Mo, 1.6 at % Si, 0.7 at % Fe, and the remainder Co; Co–Ni–Cr–Mo alloy (wrought Protasul-10, ASTM F562-84 [13]) 23 at % Cr, 36 at % Ni, 6.1 at % Mo, 1 at % Ti, 0.5 at % Fe, and the remainder Co. The pure metal components Co, Cr, Ni and Mo (all 99.9 wt %) were obtained from Metalle und Materialien GmbH, Nürnberg, Germany.

Hank's solution, a SPS contained 8 g/l NaCl, 0.40 g/l KCl, 0.35 g/l $NaHCO_3$, 0.25 g/l $NaH_2PO_4 \times 2H_2O$, 0.06 g/l $Na_2HPO_4 \times 2H_2O$, 0.19 g/l $CaCl_2 \times 2H_2O$, 0.41 g/l $MgCl_2 \times 6H_2O$, 0.06 g/l $MgSO_4 \times 7H_2O$ and 1 g/l glucose. Ethylenediaminetetraacetic acid (EDTA) disodium salt dihydrate was added, when required, to a concentration of 50 mM. Solutions were adjusted to pH 7.8. All chemicals were from Merck, Darmstadt, Germany.

The test specimens were cut into discs of 15 mm diameter. After being mechanically polished to mirror finish and rinsed with distilled water, they were embedded in a Teflon PAR holder for use as a working electrode. The reference electrode was a saturated calomel electrode (SCE, 0.242 V vs. SHE) and the counterelectrode a high purity graphite rod. Potentiodynamic curves were recorded at a scan rate of 1 mV/s using an EG&G PAR PC-controlled potentiostat/galvanostat Model 263 controlled by M352 Softcorr computer programme.

The passive layers on the alloy surface were formed under potentiostatic conditions for 1 h at potentials of -0.7, -0.3, 0.1, 0.6 and 0.8 V. These potentials were chosen with reference to the characteristic features of the polarisation curve (see Fig. 2). After the electrochemical preparation, the specimens were rinsed with distilled water, dried and transferred to the analyser chamber on the same day.

XPS measurements were performed using a VG Scientific Microlab 310F instrument using non-monochromatised Al K_α radiation ($E = 1486.6$ eV) and a hemispherical electron analyser operating at a constant transmission pass energy of 20 eV. Spectra were collected by Eclipse V 2.1. data analysis software supplied by the manufacturer. The thickness of the passive layer was determined by Argon ion sputtering for different time intervals. The reference sputtering rate was 0.01 nm/s and was calculated relative to Ta_2O_5 as the intensity of oxygen signal decrease to a half [14]. Sputter depth profiles were measured for passive films formed at two selected potentials, 0.1 and 0.6 V, for both alloys in SPS with and without 50 mM EDTA.

After background subtraction according to Shirley and processing by XFIT software developed by Wolff, the XPS signals were separated into the contributions of the different species [15]. Cr 2p, Co 2p, Ni 2p, Mo 3d, and O 1s were used as standards as published [16]. Standard binding energies of XPS peaks are presented in Table I. As standard peaks, metal samples oxidised for 1 h at the following temperatures were used: Cr at 600 °C (Cr_2O_3, CrO_3), Co at 200, 600 and 900 °C (CoO, Co_2O_3), Ni at 500 °C (NiO), and Mo at 200 °C (MoO_3). The parameters of $Cr(OH)_3$ were obtained as the difference between peaks for Cr_2O_3 and the corresponding electrochemically oxidised sample. Although the Co $2p_{1/2}$ signal is less intense than Co $2p_{3/2}$, it exhibits a larger difference between Co(II) and Co(III) species [17] and has therefore been used for data evaluation. Fig. 1 presents examples of deconvoluted spectra. To calculate the composition of the passive layer, peak areas were

TABLE I Binding energy of the standard spectra used to evaluate the oxidised samples

Binding energy (eV)		
	$2p_{1/2}$	satellite
Co(0)	793.1	
Co(II)	796.6	802.3
Co(III)	794.8	804.3
	$2p_{3/2}$	$2p_{1/2}$
Cr(0)	574.4	583.6
Cr_2O_3	756.3	585.7
$Cr(OH)_3$	577.5	587.1
Cr(VI)	578.7	588.2
	$3d_{5/2}$	$3d_{3/2}$
Mo(0)	227.9	230.9
Mo(VI)	231.5	235.3
	$2p_{3/2}$	satellite
Ni(0)	852.9	854.4
Ni(II)	859.4	855.2
	1s	
O^{2-}	530.2	
OH^-	531.4	
H_2O	532.7	

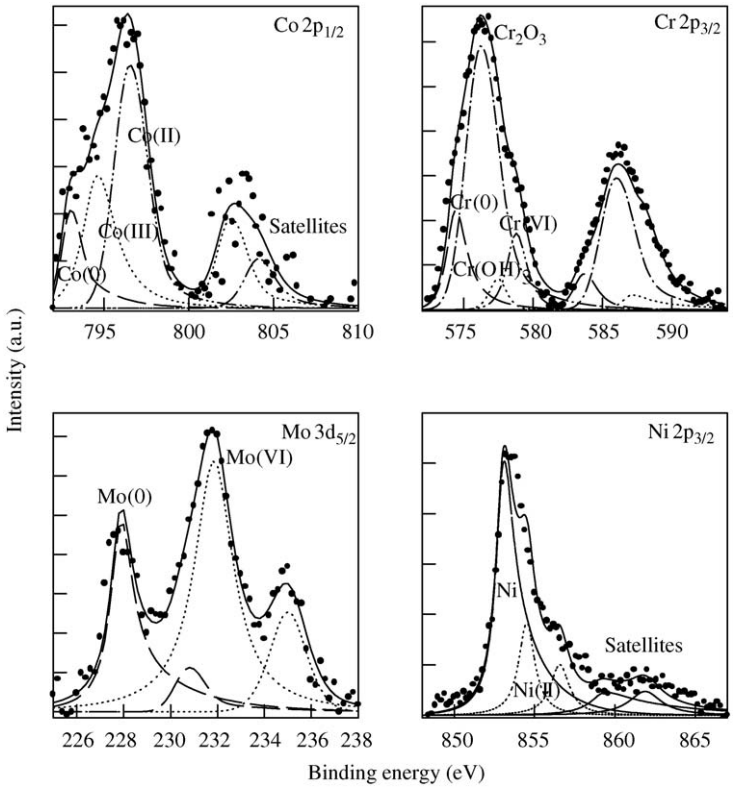

Figure 1 Examples of fitted XPS spectra for Co–Ni–Cr–Mo alloy electrochemically passivated in SPS at 0.6 V for 1 h.

corrected by the corresponding photoionisation cross-sections: $\sigma(\text{Co } 2p_{1/2}) = 6.54$, $\sigma(\text{Cr } 2p_{3/2}) = 6.90$, $\sigma(\text{Mo } 3d_{5/2}) = 5.15$, $\sigma(\text{Ni } 2p_{1/2}) = 13.04$, and $\sigma(\text{O } 1s) = 2.51$ [18, 19].

Results and discussion

The features of the potentiodynamic polarisation curves indicate the potentials at which the formation of different oxides occurs or where certain redox reactions take place. Fig. 2 shows anodic potentiodynamic curves for Co–Ni–Cr–Mo and Co–Cr–Mo alloys and their metal components in SPS with and without 50 mM EDTA. After 1 h stabilisation at the corrosion potential, E_{corr} for Co in SPS is -0.52 V, for Mo -0.32 V, for Ni -0.28 V, for Cr -0.58 V, for Co–Ni–Cr–Mo alloy -0.50 V and for Co–Cr–Mo alloy -0.55 V. Following the Tafel region, both alloys and all metals except Mo exhibit passive behaviour. The extent of the passive range differs in the order Co < Ni < Cr < both alloys. It is limited by the breakdown potential (E_b) which is defined as the potential at which the current density in the passive range starts to increase abruptly. The breakdown potential for Co in SPS is -0.25 V, for Mo 0 V and for Ni 0.12 V; Cr and the two alloys exhibit similar values of approximately 0.45 V. In the presence of EDTA, Co and Mo show no tendency to passivate, in contrast to Ni and the two alloys, whose breakdown potentials, however, are moved by approximately 0.1 V to more negative values. The current density in the passive range of Cr and the alloys is apparently unaffected by EDTA, however, it increases more steadily in the transpassive range than in SPS alone.

Fig. 3 presents Co 2p, Cr 2p and Mo 3d XPS spectra of Co–Cr–Mo alloy in SPS in dependence on the polarisation potential. In all cases, a decreasing metal signal is observed with increasing passivation potential, indicating the growth of the oxide layer. In the case of Co, formation of the oxide layer starts with the formation of Co(II) at $E \geq 0.1$ V and Co(III) at $E \geq 0.6$ V. Chromium(III) oxide and hydroxide are formed at low potentials. Cr(VI) is formed at $E \geq 0.6$ V and becomes the predominant species for $E \geq 0.8$ V. Molybdenum is oxidised at $E \geq 0.1$ V with the formation of Mo(VI) oxide.

Fig. 4 presents Co 2p, Cr 2p, Mo 3d and Ni 2p XPS spectra of Co–Ni–Cr–Mo alloy in SPS in dependence on

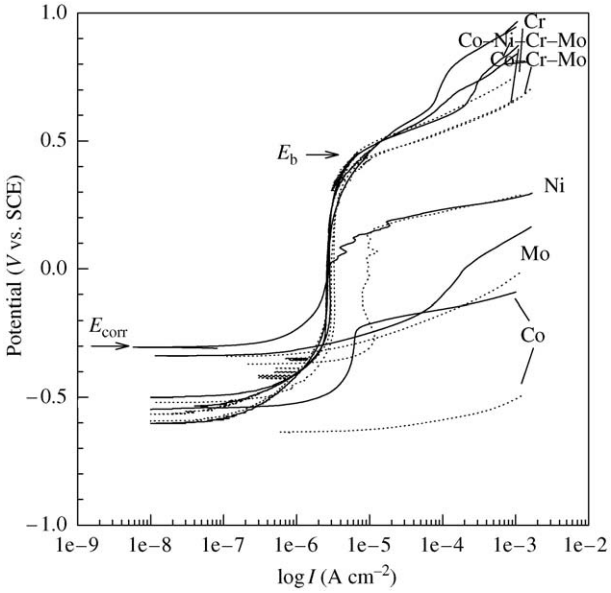

Figure 2 Potentiodynamic curves for Co–Cr–Mo and Co–Ni–Cr–Mo alloys and individual metals Co, Cr, Mo and Ni in SPS (full line) and SPS containing 50 mM EDTA (dotted line). $dE/dt = 1$ mV/s.

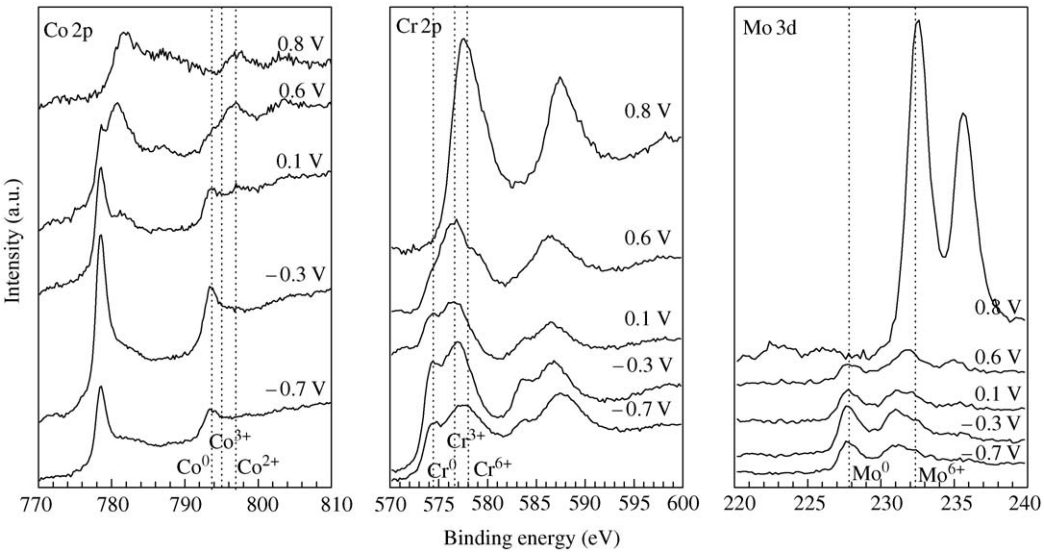

Figure 3 Normalised XPS Co 2p, Cr 2p and Mo 3d signals recorded for Co–Cr–Mo alloy after 1 h of oxidation at various electrode potentials in SPS. The positions of standard peaks are marked.

the polarisation potential. The oxidation of cobalt and molybdenum to Co(II) oxide and Mo(VI) oxides starts at more negative potentials ($E > -0.3$ V) than in the Co–Cr–Mo alloy. Chromium behaves similarly to Co–Cr–Mo alloy. The oxidation of nickel to Ni(II) oxide takes place at $E > -0.7$ V.

XPS spectra recorded in EDTA-containing SPS are qualitatively similar to those in SPS alone (Figs. 3 and 4). The main differences are that formation of the oxide layers begins at somewhat more negative potentials and that less oxide is formed. The cationic composition of the passive layers after the oxidation of the Co–Cr–Mo and Co–Ni–Cr–Mo alloys in SPS, with and without EDTA, was calculated as a function of oxidation potential (Fig. 5). The content of Cr-oxide in the passive layers formed on Co–Cr–Mo and Co–Ni–Cr–Mo alloys is up to three-fold greater than that in the bulk alloy (Fig. 5(a)). In the case of Co–Cr–Mo alloy the second major constituent of the passive layer is CoO which is, however, depleted compared to the content in the bulk alloy. The content of Mo-oxide is larger in the passive layer than in the bulk alloy. Li *et al*. obtained similar results when studying the Co–Cr–Mo alloy in biosimulating solutions using Surface-enhanced Raman Spectroscopy [12]. In the case of Co–Ni–Cr–Mo alloy, Ni-oxide becomes the second major constituent of the passive layer (Fig. 5(b)), its content in the passive layer increases above -0.3 V (Fig. 5(c)). Co-oxide is also identified but its content is much lower than in the passive layer formed on Co–Cr–Mo alloy. EDTA caused a decrease in the content of Co and Mo at potentials more positive than 0.1 V (Fig. 5(c)). Consequently, the content of chromium increases substantially in this potential range. In the case of Co–Ni–Cr–Mo alloy, a similar situation was observed (Fig. 5(d)). The decrease of the cationic content of a particular metal in the passive layer is clearly related to the stability constant of its complex with EDTA, as will be discussed below.

Figs. 6–9 show the composition of the oxide layer as a function of depth for Co–Cr–Mo and Co–Ni–Cr–Mo alloys, after oxidation at 0.1 and 0.6 V in SPS and SPS containing EDTA. Profiles present in-depth content of metallic and oxidised species of particular metal. After each sputtering step, the composition of each oxide and metal species was plotted cumulatively along the ordinate, so that the total composition amounted 100% [21]. The precise stoichiometry of the oxide cannot be determined due to ion-sputtering-induced effects, such as reduction of the oxidation state [20, 21]. The sputtering rate determined for the Ta_2O_5 standard was 0.01 nm/s. The sputter depth profile after passivation at 0.1 V in SPS shows the formation of a chromium-enriched/cobalt-depleted passive layer (Fig. 6(a)). The predominant constituent at the surface of the passive layer is Cr-oxide. The passive layer itself is constituted by Cr_2O_3, CoO and MoO_3. The position of the XPS spectra shows that cobalt oxide is present at up to 160 s of sputtering, that is up to 1.6 nm depth. Above that value, cobalt is present only as the metal species. Mo-oxide is present up to 1.2 nm depth, but only Mo metal species can be detected at deeper levels. Cr-oxide is present almost throughout the layer, that is, up to 5.2 nm.

After passivation at 0.6 V, the layer thickness increases significantly (Fig. 6(b)). After sputtering the outermost layer the content of Cr remains practically unchanged throughout the passive layer. In contrast to passivation at 0.1 V, where Co metal content increases steadily from the surface towards the bulk, it reaches a plateau between 9 and 30 nm depth after passivation at 0.6 V. Cobalt and molybdenum are present as oxides up to 12 nm, below which only cobalt and molybdenum metals can be detected. In EDTA containing SPS, there are significant differences (Fig. 7). The content of both Co- and Mo-oxides is lower after passivation at 0.1 and 0.6 V (Fig. 7(a) and (b)). After oxidation at these two potentials in EDTA-containing SPS, cobalt oxide extends to 0.4 nm and 6 nm depth respectively, which is much less than in the absence of EDTA, where CoO can be found up to 1.6 and 12 nm. Once the CoO is sputtered away, Co metal species quickly predominates in the inner part of the layer. The content of Mo-oxide is very low and can be detected up to 0.4 and 9 nm depth after passivation at 0.1

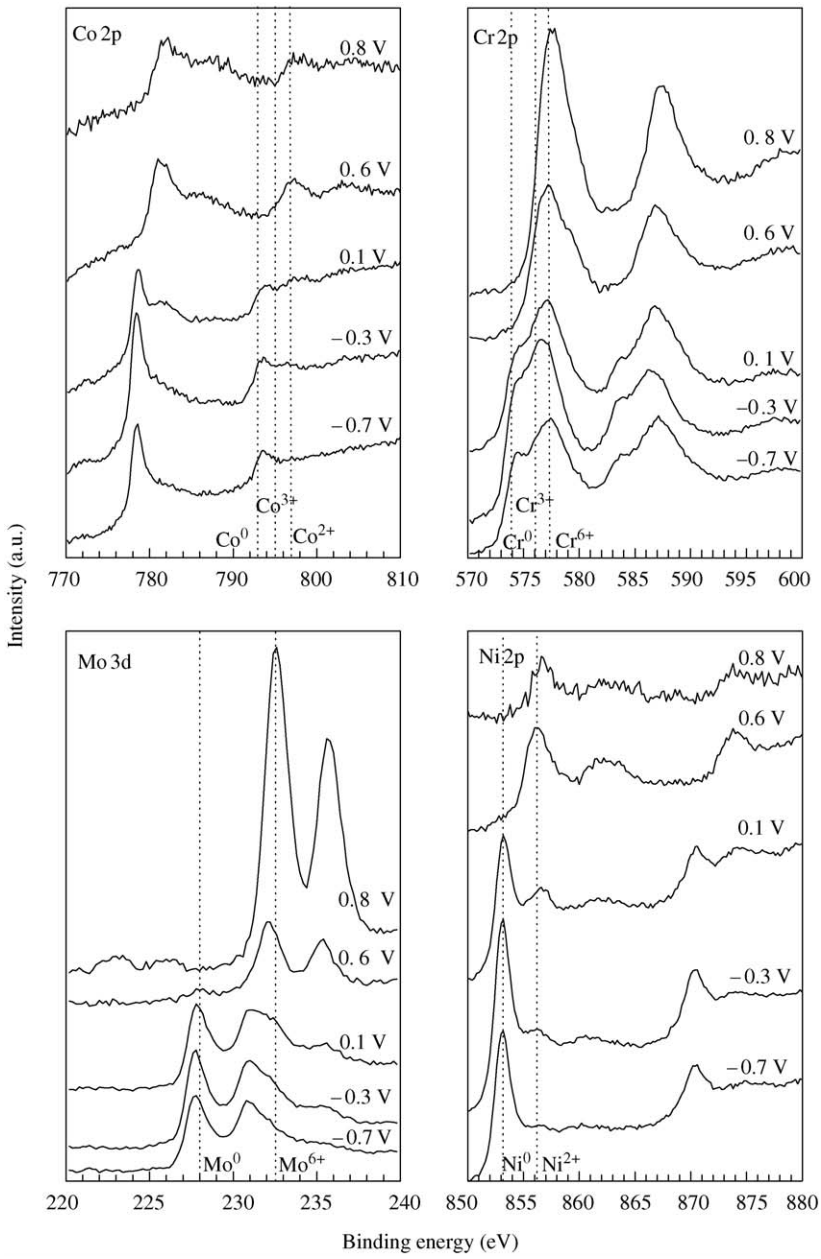

Figure 4 Normalised XPS Co 2p, Cr 2p, Mo 3d and Ni 2p signals recorded for Co–Ni–Cr–Mo alloy after 1 h of oxidation at various electrode potentials in SPS. The positions of standard peaks are marked.

and 0.6 V in EDTA-containing solution, compared to 1.2 and 12 nm, respectively, in its absence (Fig. 6). Beyond this, only Mo species can be detected. The main oxide is Cr-oxide and is present throughout the layer.

As already shown by the cationic fraction (Fig. 5), Cr-oxide is the major constituent of the passive layer on both Co–Cr–Mo and Co–Ni–Cr–Mo alloys, although its content in the latter is lower due to the formation of Ni-oxide, as well as Co-oxide (Fig. 9). The outermost part of the layer is chromium-enriched, the other three oxides being present as minor constituents. The contents of Ni, Co and Mo species increase as the oxide layer is sputtered away and bulk composition is reached. After passivation at 0.1 V, Co-, Ni- and Mo-oxides are detected up to 0.8 nm depth (Fig. 9(a)). Cr-oxide is present throughout the whole depth. After sputtering the outermost layer, the content of Cr in the passive layer formed at 0.6 V remains practically unchanged across the whole passive layer (Fig. 9(b)). Cobalt and nickel are present as oxides up to 10.5 nm, beyond which only cobalt and nickel metals can be detected. Mo-oxide can be detected up to 13.5 nm depth, beyond which only metal is present. In EDTA containing solution, after passivation at 0.1 V, Cr-oxide is detected throughout the whole depth, the other three constituents being present up to 0.8 nm. After passivation at 0.6 V, the content of Cr-oxide is considerably increased. The other three constituents, Co, Ni and Mo, are significantly depleted at the outer layers. Co-oxide is present up to 8 nm and Ni-oxide and Mo-oxides are detected up to 12 nm depth. Beyond this, only metal species are present.

Based on depth profiles including both cationic (metal) and anionic (oxygen) species, the thickness of the passive layers was calculated, relative to Ta_2O_5, as the point at which the intensity of the oxygen signal has decreased to a half [14]. The thickness of the layer formed on Co–Cr–Mo alloy in SPS after passivation at 0.1 V is 2.1 nm, and at 0.6 V 13.5 nm. In the presence of EDTA the passive layer becomes thinner, that is 1.6 nm at 0.1 V, and 7.5 nm at 0.6 V. For Co–Ni–Cr–Mo alloy the thickness of the

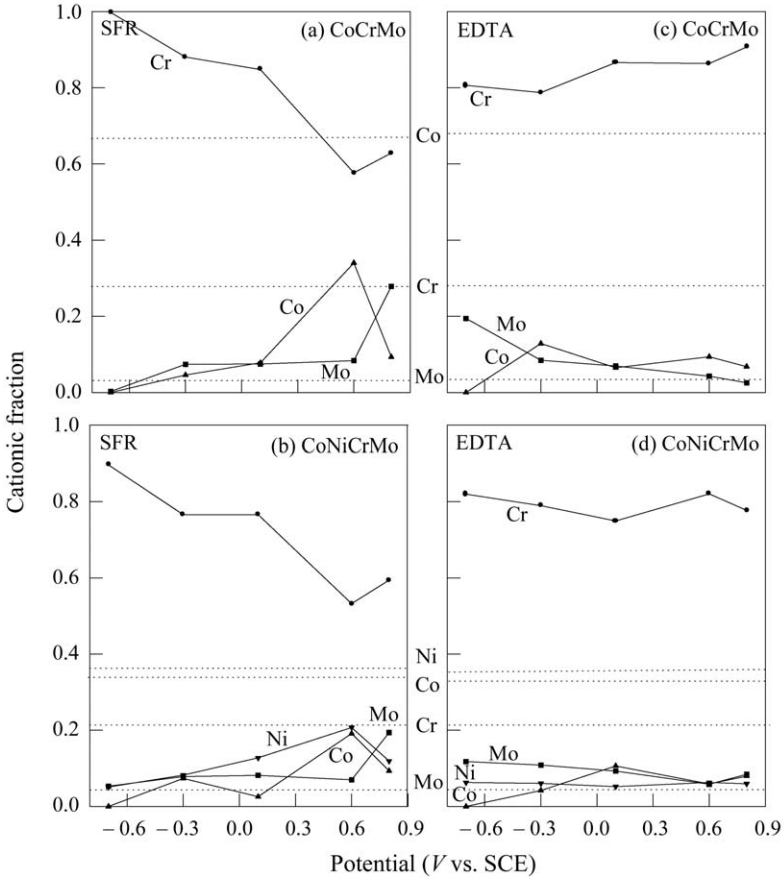

Figure 5 Cationic composition of the passive layer after oxidation of Co–Cr–Mo and Co–Ni–Cr–Mo alloy in SPS (a, b) and SPS containing 50 mM EDTA (c, d) as a function of oxidation potential. Dotted lines denote the atomic fractions for particular metal component in the bulk alloy.

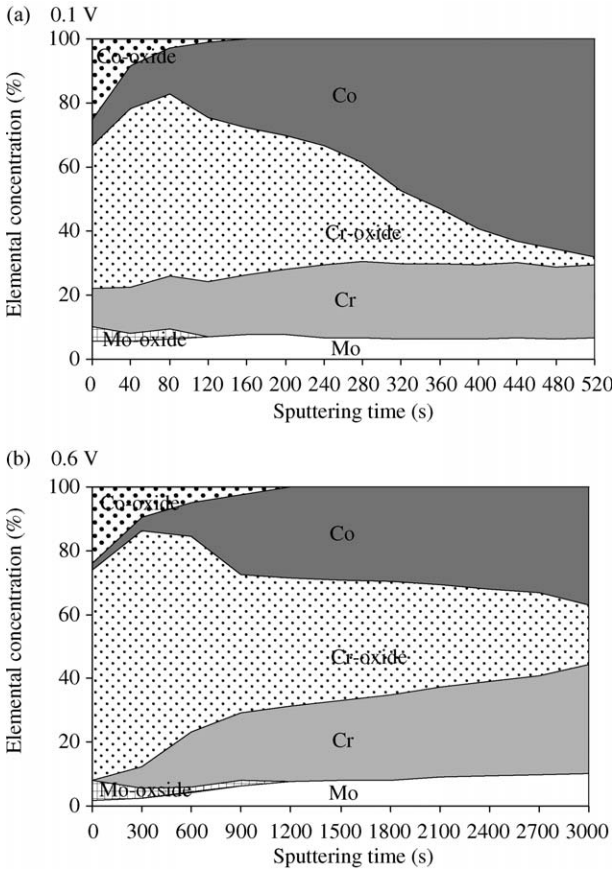

Figure 6 Depth profiles of Co–Cr–Mo alloy after oxidation at (a) 0.1 V and (b) 0.6 V for 1 h in SPS as a function of sputtering time. Sputtering rate relative to Ta_2O_5 is 0.01 nm/s.

passive layer is less than that of the Co–Cr–Mo alloy in both solutions and at both passivation potentials. The thickness in SPS at 0.1 V is 1.7 nm, and at 0.6 V 10.5 nm, whereas in the presence of EDTA the thickness is only

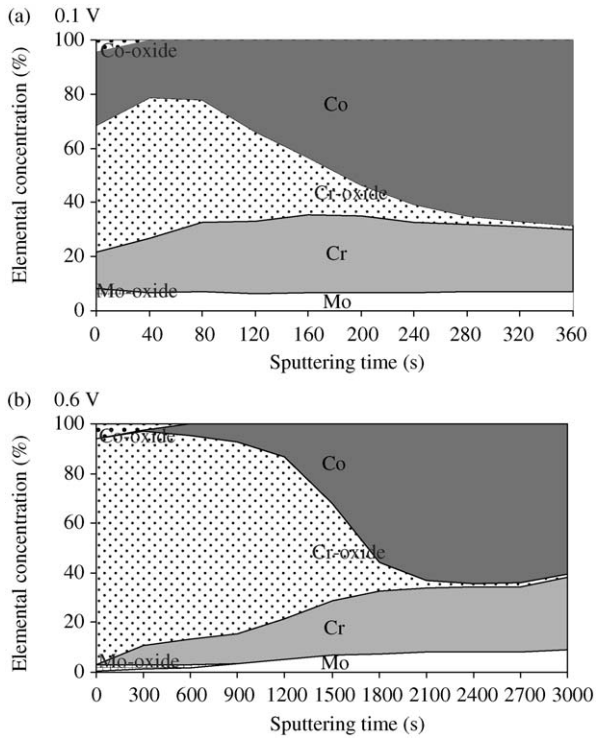

Figure 7 Depth profiles of Co–Cr–Mo alloy after oxidation at (a) 0.1 V and (b) 0.6 V for 1 h in SPS containing 50 mM EDTA as a function of sputtering time. Sputtering rate relative to Ta_2O_5 is 0.01 nm/s.

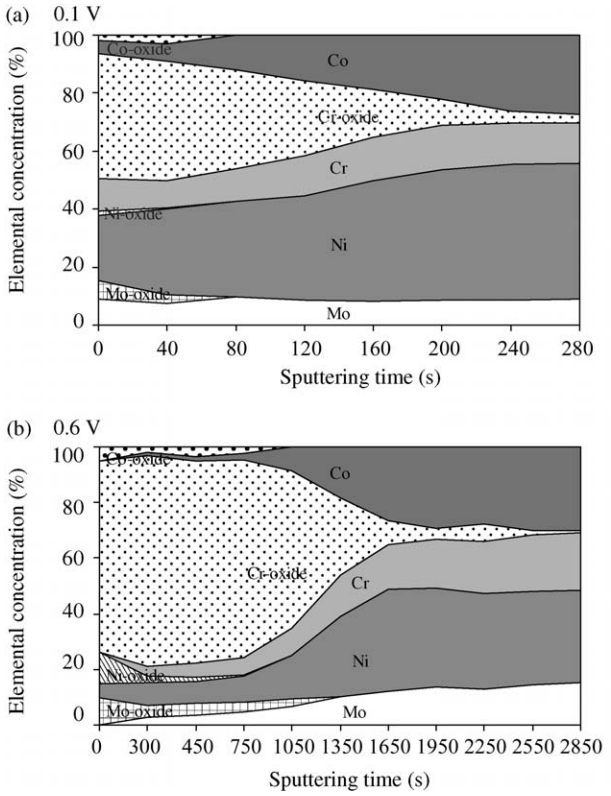

Figure 8 Depth profile of Co–Ni–Cr–Mo alloy after oxidation at (a) 0.1 V and (b) 0.6 V for 1 h in SPS as a function of sputtering time. Sputtering rate relative to Ta_2O_5 is 0.01 nm/s.

1.4 nm at 0.1 V, and 6.9 nm at 0.6 V. The thickness of the passive film is thus strongly affected by the complexing agent, owing to the possibility of complexation reactions [22]. Ni and Co form strong complexes with EDTA, with

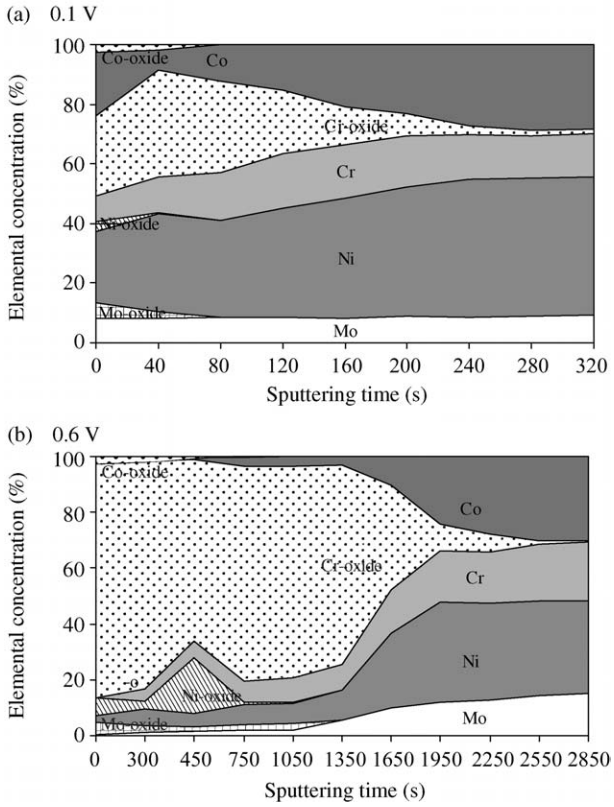

Figure 9 Depth profile of Co–Ni–Cr–Mo alloy after oxidation at (a) 0.1 V and (b) 0.6 V for 1 h in SPS containing 50 mM EDTA as a function of sputtering time. Sputtering rate relative to Ta_2O_5 is 0.01 nm/s.

logarithm of stability constant ($\log K_{st}$) of 16.3 for Co^{2+}, 41.4 for Co^{3+} and 18.5 for Ni^{2+} [23]. Instead of being incorporated in the passive layer, therefore, Co and Ni species may be further complexed by EDTA, due to the large value of $\log K_{st}$. No data exist for stability constants for complexes of Mo with EDTA, but a similar effect is observed in those for Co and Ni. EDTA can form very strong complexes with Cr^{3+} ions [23], but due to the very slow dissolution of the strongly protective Cr_2O_3 layer, the amount of Cr(III) species available for complexing is small [24].

Conclusions

The composition, thickness and depth profiles of the oxide films formed on Co–Cr–Mo and Co–Ni–Cr–Mo alloys were studied by XPS analysis in simulated physiological solution with and without EDTA at pH = 7.8. The electrochemical results show that both Co-based alloys passivate very well in simulated physiological solution. Their electrochemical characteristics are similar to those of chromium metal, leading to the assumption that Cr-oxide would be the major constituent of the passive film formed on these alloys. This hypothesis is confirmed by the XPS measurements. The sputter depth profiles prove the formation of a chromium-enriched/cobalt-depleted passive layer on Co–Cr–Mo alloy and a chromium-enriched/nickel- and cobalt-depleted passive layer on Co–Ni–Cr–Mo alloy. Cr-oxide is the major constituent of the passive layer on the Co–Cr–Mo and Co–Ni–Cr–Mo alloys, despite the fact that, considering the atomic composition, it is only the second and third metal component, respectively, of the bulk alloys. Mo-oxide is in both cases present as a minor constituent of the passive layer. All three minor constituents, that is Co-, Ni-, and Mo-oxides are present primarily in the outer part of the layer.

The complexing agent, EDTA, affects the passivation of both alloys. Cobalt, molybdenum and nickel are depleted throughout the passive layer due to the preferential dissolution at the oxide/electrolyte interface and the complexing of metal cations by EDTA. Thus the stability of the passive layer is lower in the presence of complexing agent in the solution.

References

1. H. B. SKINNER, in ''Current Diagnosis and Treatment in Orthopedics'' (Norwalk, Connecticut, Appleton and Lange, 1995) p. 19.
2. H. G. WILLERT, G. H. BUCHHORN and M. SEMLITSCH, in ''Biological Material, and Mechanical Considerations of Joint Replacement'' (Raven Press, New York, 1988) p. 129.
3. R. M. URBAN, J. J. JACOBS, M. J. TOMLINSON, J. GAVRILOVIC, J. BLACK and M. PEOCH, *J. Bone Joint Surg.* **82** (2000) 457.
4. N. HALLAB, K. MERRIT and J. J. JACOBS, *ibid.* **83A** (2001) 428.
5. J. J. JACOBS, A. SKIPOR, P. DOORN, P. CAMPBELL, T. P. SCHMALZRIED, J. BLACK and H. C. AMSTUTZ, *Clin. Orthop. Rel. Res.* **329S** (1996) 256.
6. W. BRODNER, P. BITZAN, V. MEISINGER, A. KAIDER, F. GOTTSAUNER-WOLF and R. KOTZ, *J. Bone Joint Surg.* **78B** (1997) 316.
7. T. HANAWA, S. HIROMOTO and K. ASAMI, *Appl. Surface Sci.* **183** (2001) 68.

8. R. L. MOORE, G. L. GROBE III and J. A. GARDELLA, *J. Vac. Sci. Technol.* **A9** (1991) 1323.
9. C. MAFFIOTTE, M. NAVAS, M. L. CASTAÑO and A. M. LANCHA, *Surf. Interface Anal.* **30** (2000) 161.
10. G. LARRAMONA and C. GUETIERREZ, *J. Electroanal. Chem.* **293** (1990) 237.
11. A. BEWICK, C. GUETIERREZ and G. LARRAMONA, *ibid.* **333** (1992) 165.
12. Y. S. LI, K. WANG, P. HE, B. X. HUANG and P. KOVACS, *J. Raman Spectrosc.* **30** (1999) 91.
13. Annual Book of ASTM Standards, ''Medical Devices'', vol. 13.01 (Philadelphia, ASTM, 1988).
14. S. HOFFMAN, in ''Practical Surface Analysis'' (Wiley and Sons, Chichester, 1990) p. 141.
15. M. WOLFF, Ph.D. thesis, Heinrich-Heine University, Düsseldorf, Germany, 1992.
16. I. MILOŠEV and H.-H. STREHBLOW, *Electrochim Acta* **48** (2003) 2767.
17. A. FOELSKE and H.-H. STREHBLOW, *Surf. Interface Anal.* **29** (2000) 548.
18. J. H. SCOFIELD, *J. Electron Spectrosc. Relat. Phenom.* **8** (1976) 129.
19. R. F. REILMAN, A. MSEZANE and S. T. MANSON, *J. Electron Spectrosc. Relat. Phenom.* **8** (1976) 389.
20. W. H. HOCKING, F. W. STANCHELL, E. MCALPINE and D. H. LISTER, *Corros. Sci.* **25** (1985) 531.
21. N. S. MCINTYRE, D. G. ZETARUK and E. V. MURPHY, *Surf. Interface Anal.* **1** (1979) 105.
22. I. MILOŠEV, *J. Appl. Electrochem.* **32** (2002) 311.
23. R. M. SMITH and A. E. MARTELL, in ''Critical Stability Constants'', vol. 3 (New York/London, Plenum Press, 1977).
24. A. KOCIJAN, I. MILOŠEV and B. PIHLAR, *J. Mater. Sci.: Mater. Med.* **14** (2003) 69.

Received 12 November 2003
and accepted 10 February 2004